Geophysical Research Letters

RESEARCH LETTER
10.1029/2018GL081704

Time of Steady Climate Change

Megan Lickley[1], b. b. cael[2], and Susan Solomon[1]

[1]Department of Earth, Atmospheric, and Planetary Sciences, Massachusetts Institute of Technology, Cambridge, MA, USA, [2]Department of Oceanography, School of Ocean and Earth Science and Technology, University of Hawai'i at Mānoa, Honolulu, HI, USA

Key Points:
- The stabilization of greenhouse gas concentrations would lead to regional differences in the time of achieving steady temperature increases
- The use of General Circulation Model ensembles allows evaluation of the relative timing of arriving at a state of steady climate change
- The Time of Steady Change occurs latest in low latitudes and the Arctic despite these areas steadying at very different warming rates

Supporting Information:
- Supporting Information S1

Correspondence to:
M. Lickley,
mlickley@mit.edu

Citation:
Lickley, M., cael, b. b., & Solomon, S. (2019). Time of steady climate change. *Geophysical Research Letters*, *46*, 5445–5451. https://doi.org/10.1029/2018GL081704

Received 15 DEC 2018
Accepted 10 APR 2019
Accepted article online 16 APR 2019
Published online 17 MAY 2019

Abstract Under an emission scenario where atmospheric greenhouse gas concentrations are stabilized, previous work suggests that on centennial time scales the rate of global temperature increases would steady at significantly lower rates than those of the 21st century. As climate change is not globally uniform, regional differences in achieving this steady rate of warming can be expected. Here, we define a "Time of Steady Change" (TSC) as the time of reaching this steady rate of warming, and we present a method for estimating TSC with the use of General Circulation Model experiments run under greenhouse gas stabilization scenarios. We find that TSC occurs latest in low latitudes and in the Arctic, despite these areas steadying at very different absolute warming rates. These broad patterns are robust across multiple General Circulation Model ensembles and alternative definitions of TSC. These results indicate large regional differences in the trajectory of climate change in coming centuries.

Plain Language Summary In a future where greenhouse gas concentrations have been stabilized, it is expected that the rate of global warming will decrease to a steady and slower rate than that observed in the 21st century. We also expect that the time of arriving at this steady, slow state of warming will have regional differences with some locations steadying sooner than others. Here we examine the time it takes to arrive at this steady state of warming and probe the regional differences in this arrival time. To do so, we make use of a collection of climate models all run under identical emission scenario where the concentrations of greenhouse gases increase throughout the 21st century and are then held constant for the following two centuries. We observe regional differences in the time it takes to arrive at a slower, steady state of warming. In particular, the Arctic and tropics are the last to arrive at a steady warming rate. Because the climate signal has been found to first emerge in the tropics, this work suggests that low latitudes will experience the longest duration of rapid warming.

1. Introduction

While the Paris agreement sets an explicit goal of limiting global warming to 2°C or 1.5°C (Article 2), it also targets balancing anthropogenic sources and sinks of greenhouse gases (GHG) by participating nations in the second half of this century (Article 4). Scholars have offered various interpretations of the policy language of Article 4 of the Paris agreement. Although several interpretations are possible (Falkner, 2016; Fuglestvedt et al., 2018), we interpret the "balance of anthropogenic sources and removals by sinks of GHG" (UNFCCC, 2015) to imply eventual stabilization of atmospheric GHG concentrations.

If the stabilization of atmospheric GHG concentrations occurs, theory and modeling experiments indicate that on centennial time scales the rate of global temperature increases would steady at significantly lower rates than those of the 21st century (Hansen et al., 1985; Meehl et al., 2005; Wigley, 2005). Such scenarios suggest three stages to the anthropogenic fingerprint on global temperatures: (1) a period with an anthropogenic climate signal that cannot be detected due to climate variability being larger than the signal, (2) a period of detectable and strongly increasing transient change as a result of increasing forcing, and (3) a period of slower steady changes for near constant forcing. The focus has thus far been on the time of emergence (ToE) of anthropogenic warming, which quantifies the transition between the first two stages (Diffenbaugh & Scherer, 2011; Hawkins & Sutton, 2012; Mahlstein et al., 2011) while the time of transition between the latter two has not been probed. Here, we define a "Time of Steady Change" (TSC) as the time of reaching the third stage, which, together with ToE, provides a framework to quantify the duration of the period of rapid climate change (stage 2). This has important implications for understanding regional differences in the trajectory of climate change. While the rate of warming during the period of high transience has more

immediate implications for adaptation, this transition from stage 2 to stage 3 is key to the United Nations Framework Convention on Climate Change (UNFCCC) objective of avoiding dangerous interference with the climate system (which remains relevant under the Paris agreement; Jacquet & Jamieson, 2016), since, for example, a longer period of rapid warming represents a greater challenge to ecosystem adaptation. Moreover, an improved understanding of this transition time will inform decision makers, such as water resource planners, where climate uncertainty has important implications for large-scale infrastructure investments over long lifetimes such as dams (Hallegatte, 2009; Keller et al., 2004).

We define TSC as the time when the warming rate is undetectably different from that which we anticipate continuing for centuries (see Figure 1a and section 2). This demarcates the transition between the period of high transience in which rapid warming accompanies increasing GHG concentrations (Rogelj et al., 2012) and the period of steady change in which constant GHG concentrations lead to a significantly reduced rate of sustained warming (Gillett et al., 2011).

While the ToE literature has identified regions where the anthropogenic signal will be first detectable (Hawkins & Sutton, 2012; Mahlstein et al., 2011), TSC provides a framework to characterize the length of time required to transition to a near-constant climate state as GHG approach stabilization and to identify the regional disparities in the timing of this transition.

The remainder of this paper is organized as follows: In section 2 we describe the methods for quantifying TSC. Section 3 provides a summary of General Circulation Model (GCM) data sets used to quantify TSC. In section 4 we present the results of our analysis and section 5 provides a summary.

2. Methods

2.1. TSC Estimation Framework

Suppose GHG concentrations continue to increase until year 2000 + N, after which GHG concentrations stabilize and are held constant for centuries. We let m_t be the rate of warming at year t and assume that at some point following 2000 + N, warming slows to a steady rate, $m_{\text{end}} \pm \epsilon$, that continues for centuries. TSC is then defined as the first of k consecutive years in which $m_t \leq m_{\text{end}}+\epsilon$.

2.2. Estimating Rates

Due to natural variability in the climate system, background noise can obscure the warming signal, especially at small spatial scales. Therefore, to estimate a robust warming rate, we first average the annual mean temperature over a 5° × 5° grid cell resolution. Note that other spatial scales of aggregation have been tested with aggregation over larger spatial scales leading to smaller values in ϵ (e.g., see Figure 1a for globally averaged rates and Figure S2 in the supporting information (SI) for rates averaged over 20° × 20° grid cell). Warming rates for each grid cell and each GCM are then estimated over a 50-year moving window using a modified version of the Theil-Sen bootstrap estimator (Sen, 1968): 10,000 pairs of points at least 10 years apart are uniformly randomly sampled from the 50-year window. We exclude pairs within 10 years so that the sampled distribution of the warming rate reflects warming over decadal and longer time scales. A sample size of 10,000 pairs of points was chosen for consistency across simulations. The median slope of the 10,000 pairs is the estimated warming rate for the year in the center of the 50-year window. A 50-year window was chosen because it was the smallest window that produced similar estimates of TSC moving both forward in time and backward in time. Rates are then smoothed using a 10-year moving average. This results in yearly estimated warming rates for 2031–2275 and 2036–2275 for the Coupled Model Intercomparison Project Phase 3(CMIP3) and CMIP5 ensembles, respectively.

2.3. Estimating TSC With GCM Ensembles

We apply the TSC estimation framework to GCM simulations as follows: m_t is the multimodel median (MMM) warming rate for year t, m_{end} is the MMM rate of warming averaged over the 23rd century (i.e., for rates between 2201 and 2275). The value ϵ quantifies the multimodel standard deviation of m_{end}. We select k to be 20 years to account for multidecadal oscillations that may affect the robustness of TSC. With this selection, the earliest value of TSC could be 2051 and 2056 for CMIP3 and CMIP5, respectively.

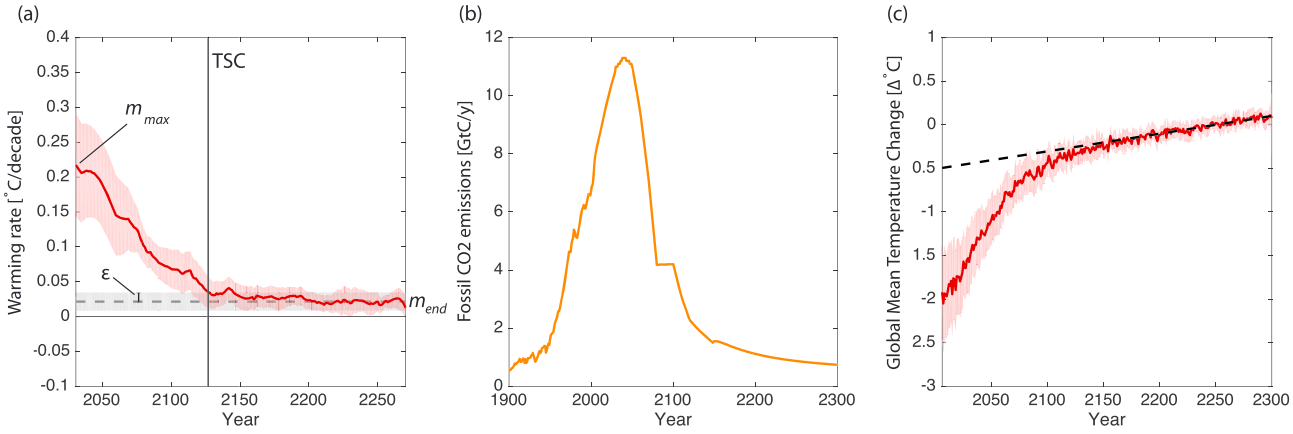

Figure 1. (a) Framework for estimating the Time of Steady Change (TSC) using the example of global mean surface warming rates from the Representative Concentration Pathway 4.5 (RCP4.5) ensemble. The solid red line indicates the multimodel median (MMM) warming rate over time, and the red-shaded region indicates the range of uncertainty (±1 multimodel standard deviation). $m_{\max}$ is the maximum warming rate in the 21st century. The dotted gray line is the MMM 23rd century warming rate (m_{end}), and the gray-shaded region ($\pm\epsilon$) indicates one multimodel standard deviation around m_{end}. The vertical line centered around the year 2127 is the estimated TSC as it coincides with the first of at least 20 consecutive years in which the solid red line falls within 1ϵ of m_{end}. (b) The RCP 4.5 Fossil CO_2 extended stabilization emission scenario (Meinshausen et al., 2011). CO_2 emissions peak in the year 2040, and by mid-22nd century they have reduced to below 1950 emissions values. (c) The RCP 4.5 MMM global mean absolute temperature change relative to 2201–2300 with ±1 multimodel standard deviation shown in red. The black dotted line indicates the MMM global mean temperature trend over 2201–2300, estimated using linear regression.

3. Data

To assess TSC, we employ GCM ensembles, which contain idealized experiments of the evolution of the climate system under prescribed emissions trajectories. Because GCM ensembles include simulations from multiple GCMs, they allow us to quantify uncertainty in future climate change due to internal variability of the climate system and model uncertainty (Deser et al., 2012; Thompson et al., 2015). To estimate TSC, certain characteristics are required. First, GCMs must be forced by an emission scenario that results in increasing GHG concentrations until a certain time, followed by constant GHG concentrations. Second, after GHG concentrations are held fixed, GCMs must continue to be run for at least another century, preferably longer, in order for the climate system to adjust to a near-stable warming rate. And third, there must be a sufficiently large number of ensemble members available in order to robustly define uncertainty in the particular ensemble.

The CMIP5 and CMIP3 archives contain three GCM "constant composition commitment" experiments that emulate the stabilization of GHG as described above (Meehl et al., 2007; Meinshausen et al., 2011). In the CMIP5 experiment, GCMs are forced by the Representative Concentration Pathway 4.5 (RCP4.5) from 2005 to 2150, after which point the GHG composition of the atmosphere is held constant and models are run out to 2300 (Figure 1b). In the CMIP3 experiments, GCMs are forced by either the SRES B1 or A1B emission scenarios from 2000 to 2100, after which point the GHG composition of the atmosphere is held constant and models are run out to 2300 (Meehl et al., 2007). For all three emission scenarios considered here, peak GHG concentrations occur at their stabilization values. Of the RCP4.5, A1B, and B1 experiments, we have obtained 10, 11, and 17 GCM simulations, respectively. TSC is estimated from mean annual surface temperature fields from these experiments (section 2). The list of model simulations for each ensemble is provided in the SI.

4. Results

Here we present the results from RCP4.5; results from CMIP3 are included in the SI and exhibit similar spatial patterns of TSC, demonstrating that these patterns are insensitive to the specific scenario, at least across this set of available options.

For the CMIP5 ensemble, Figure 1 shows the global TSC to be 2127, with a bootstrap standard error of 10.9 years. This indicates that for the RCP 4.5 scenario, it takes the models approximately a century after peak GHG emissions to reach a steady rate of warming. Note, however, that we would expect TSC to

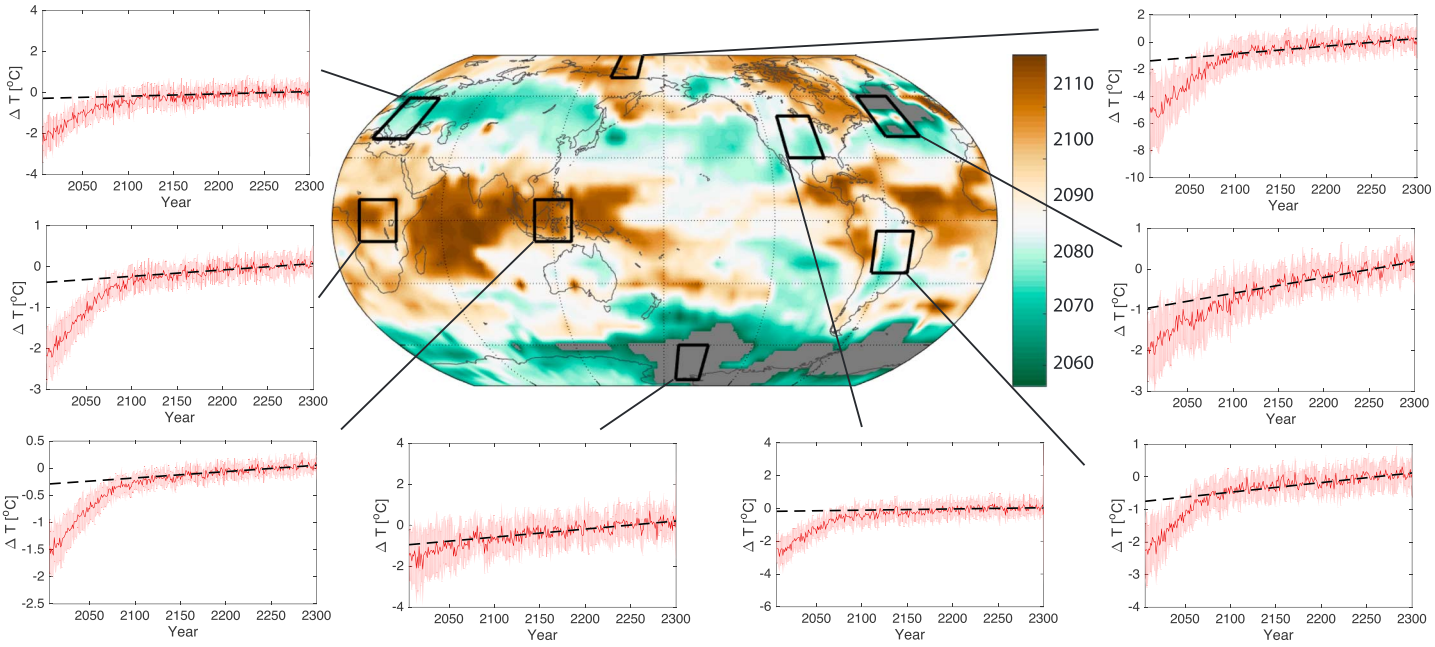

Figure 2. The Time of Steady Change estimated using the Representative Concentration Pathway 4.5 ensemble. The color bar indicates the year in which the multimodel mean warming rate is within uncertainty of 23rd century warming rates. Line plots are as Figure 1c for selected 20° × 20° grid boxes. Note the relatively large uncertainties in model temperature change in the high-latitude grid boxes relative to the low-latitude grid boxes. An analogous figure with line plots showing warming rates as in Figure 1a is provided in the supporting information.

occur sooner for a scenario where GHG concentrations stabilize faster after peak emissions (Ricke & Caldeira, 2014) or for zero emissions (e.g., Solomon et al., 2009). The global TSC for the A1B and B1 scenarios are 2150 (SE = 16.3 years) and 2107 (SE = 10.8 years), respectively. TSC values for individual GCMs using an alternative method are shown in the SI.

Figure 2 shows the geographical distribution of TSC for the CMIP5 ensemble. The latest TSCs are mostly found in the Arctic and low latitudes, the earliest TSCs in the Northern North Atlantic (NNA) and Southern Ocean, with intermediate and variable TSCs in midlatitudes. These broad patterns are consistent with the CMIP3 ensembles (shown in the SI). Figure 1 and Figure S2 in the SI illustrate that the TSC for the globally averaged rate of warming is later than most regions because it exhibits less uncertainty and variability than warming rates at smaller spatial scales (Hawkins & Sutton, 2012); the area-weighted average TSC (at the 5° × 5° spatial resolution considered here) is 2090, and the latest TSC estimated for any one 5° × 5° grid box is 2124.

Regional differences in TSC depend not only on the relative difference in warming rates between the 21st and 23rd centuries but also on the uncertainty or variability in the future mean warming rates. The relationship between these two factors is analogous to a signal-to-noise ratio, where the "signal" is the difference between the maximum 21st century MMM warming rate (m_{max}) and the 23rd century MMM warming rate (m_{end}) and the "noise" is the internal climate variability or uncertainty, quantified by ϵ, the multimodel standard deviation in m_{end}. We define a signal-to-noise ratio $\xi = (m_{max} - m_{end})/\epsilon$ (Figure 3a). Globally, ξ and TSC are correlated (Spearman correlation of 0.74, $p << 0.01$), showing that ξ exerts a strong influence on TSC. While m_{end} is enhanced at higher latitudes (Figure 3b), the signal ($m_{max} - m_{end}$) is largely dominated by m_{max} and thus by the land-sea warming contrast (Manabe et al., 1991; Sutton et al., 2007) and Arctic amplification (Bekryaev et al., 2010; SI). Similar to m_{end}, ϵ exhibits higher values in higher latitudes, influenced in part by the Atlantic Multidecadal Oscillation (Knight et al., 2006; Figure 3c).

5. Discussion and Conclusions

The factors determining TSCs differ from region to region. Between the regions with the latest TSCs, all of m_{max}, m_{end}, and ϵ exhibit greater magnitudes in the Arctic than in low latitudes. While these regions display

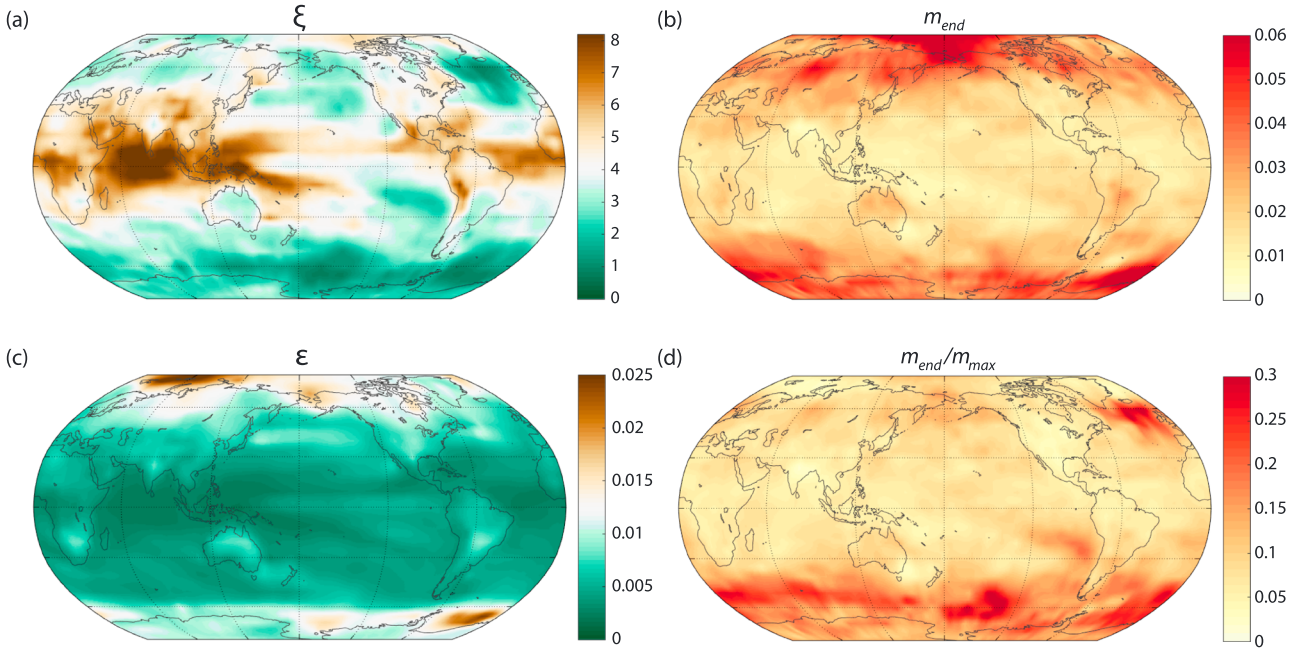

Figure 3. (a) Map of the Representative Concentration Pathway 4.5 (RCP4.5) multimodel mean (MMM) value of $\xi = \frac{m_{\max} - m_{\text{end}}}{\epsilon}$, where $m_{\max}$ is the 21st century maximum MMM warming rate, m_{end} is the 23rd century MMM warming rate, and ϵ is the multimodel standard deviation of m_{end}. (b) Map of the RCP4.5 MMM value of m_{end} in degrees Celsius per decade. (c) Map of the Coupled Model Intercomparison Project Phase 5 RCP4.5 MMM value of ϵ. (d) Map of the RCP4.5 MMM value of $\frac{m_{\text{end}}}{m_{\max}}$.

similar signal-to-noise ratios, the Arctic steadies at a much higher 23rd century warming rate. Low latitudes take a similarly long time to reach steady change but stabilize at a low m_{end}.

Similarly, the NNA and the Southern Ocean exhibit early TSCs and low signal-to-noise ratios, but both ($m_{\max} - m_{\text{end}}$) and ϵ are larger in the Southern Ocean than in the NNA. Portions of the NNA and Southern Ocean have such pronounced internal variability that the MMM warming through the entire simulation period is within uncertainty of the 23rd century warming rates. These correspond with regions that have $\xi \approx 1$ or less. As expected, the areal extent of such regions is greater in the lowest-emission scenario considered here, that is, experiment B1 (SI). The early TSCs found in the Southern Ocean and NNA correspond with high $m_{\text{end}}/m_{\max}$ ratios (Figure 3d), that is, the highest 23rd century warming rates relative to maximum warming rates, meaning that models project these regions' long-term warming rates will be globally the most similar to their 21st century rates. This reflects the delayed warming in the Southern Ocean and NNA, which is understood to be driven by ocean circulation (Marshall et al., 2015). Previous studies have shown that the Southern Ocean responds as a passive tracer to anthropogenic forcing due to northward ocean heat transport and upwelling of deep ocean water in the region (Armour et al., 2016), whereas the depressed warming in the NNA has been attributed to the meridional ocean heat flux carrying more heat out of the region than into the region (Marshall et al., 2015). The ubiquitously large noise terms (i.e., ϵ) in high latitudes of the Southern Hemisphere may be, in part, a manifestation of the response of the Antarctic Oscillation to this GHG scenario, where northern high latitudes warm faster than southern high latitudes during transient periods followed by a reversal of the trend during stabilization of GHG (Cai et al., 2003).

The spatial patterns for each variable shown in Figure 3 are consistent with those from the CMIP3 ensembles (SI); however, the A1B scenario produces larger ξ and m_{end} values, globally, reflecting the long-term persistent effects of a higher emission scenario.

Of the emission scenarios considered in this analysis, higher emission scenarios coincide with later global TSC values. This could be a result of higher GHG requiring more time to reach an equilibrium warming rate or could be due to the different transition times between peak emissions and constant (or near constant) GHG. For example, a more abrupt change point from increasing to constant forcing could lead to a

delayed transition between the fast and slow climate responses following GHG stabilization (Held et al., 2010). Changes in ocean circulation provide a possible explanation of this transition time between the fast and slow response of warming (Rugenstein et al., 2016; Stouffer, 2004). Abrupt increases in forcing lead to faster relative warming of the ocean surface, increasing stability, and temporary weakening of the Atlantic meridional overturning circulation. This, in turn, leads to temporary increases in Arctic ice formation, which delays the onset of the slow increase in warming. Further experimental analysis would be required to probe the mechanisms leading to the different TSC time scales across emission scenarios.

While studies characterizing the period of steady change have primarily focused on globally averaged temperature change (Gillett et al., 2011; Meinshausen et al., 2011; Solomon et al., 2009) or spatial warming patterns over millennial time scales (Gillett et al., 2011), here we have introduced the first framework for estimating the timing of transition into this period. Just as in studies of ToE, other definitions are possible and future studies may well probe alternative definitions. While we have focused our analysis on the geographic patterns of TSC as it pertains to annual mean temperature, it is likely that the timing and spatial patterns of TSC would differ for other variables. For instance, TSC for annual rainfall is likely to be determined by large-scale circulation and changes in horizontal temperature gradients as opposed to local temperatures alone (Byrne & O'Gorman, 2015; Chadwick et al., 2013).

We have presented one formulation of this transition time, and we also explore some alternative definitions that produce similar results (SI). Even in a scenario such as RCP 4.5, where emissions are rapidly reduced by mid-21st century, there are substantial spatial differences in the time it takes to reach a rate of steady warming. This transition time occurs latest in the Arctic and low latitudes; as low latitudes have been characterized as having the earliest ToE (Hawkins & Sutton, 2012; Mahlstein et al., 2011), this study finds that they will also experience among the longest periods of high transience. While the ToE and TSC bookend this second stage of high transience, it is important to note that TSC need not imply climate stabilization. For example, amplified warming in high latitudes is expected in the 23rd century at rates that are multiple times higher than the global average of 0.02°C/decade (Figure 3b), and global mean surface temperature is expected to continue to increase for centuries under an increased constant GHG concentration scenario (Rugenstein et al., 2016; Figure 1a). Even in comparison with 21st century warming rates, relatively high rates of continued warming are expected for some regions, such as parts of the Southern Ocean and Antarctica (Figure 3d).

If the UNFCCC's objective of stabilizing GHG is achieved, then despite slower global warming rates our work suggests regional differences in the climate change trajectory in the coming centuries. An important limitation of our analysis is that TSC is estimated relative to 23rd century warming rates. This is because the ensemble simulations did not extend beyond 2300. It is possible that these rates will change in future centuries, which would result in later TSC values than the ones estimated in this analysis.

Acknowledgments
We acknowledge the World Climate Research Programme's Working Group on Coupled Modelling, which is responsible for CMIP, and we thank the climate modeling groups (listed in the SI) for producing and making available their model output. For CMIP the U.S. Department of Energy's Program for Climate Model Diagnosis and Intercomparison provides coordinating support and led development of software infrastructure in partnership with the Global Organization for Earth System Science Portals. M. L. was partly supported by a Callahan-Dee fellowship at MIT. B. C. acknowledges support from the National Aeronautics and Space Administration (grant NNX16AR47G). All GCM data used in this work are available at https://esgf-node.llnl.gov/projects/esgf-llnl/. All codes used in this work are available upon request from M. L. (mlickley@mit.edu).

References

Armour, K. C., Marshall, J., Scott, J. R., Donohoe, A., & Newsom, E. R. (2016). Southern Ocean warming delayed by circumpolar upwelling and equatorward transport. *Nature Geoscience*, *9*(7), 549–554. https://doi.org/10.1038/ngeo2731

Bekryaev, R. V., Polyakov, I. V., & Alexeev, V. A. (2010). Role of polar amplification in long-term surface air temperature variations and modern arctic warming. *Journal of Climate*, *23*(14), 3888–3906. https://doi.org/10.1175/2010JCLI3297.1

Byrne, M., & O'Gorman, P. a. (2015). The response of precipitation minus evapotranspiration to climate warming: Why the "'wet-get-wetter, dry-get-drier'" scaling does not hold over land. *Journal of Climate*, *28*(20), 8078–8092. https://doi.org/10.1175/JCLI-D-15-0369.1

Cai, W., Whetton, P. H., & Karoly, D. J. (2003). The response of the Antarctic Oscillation to increasing and stabilized atmospheric CO2. *Journal of Climate*, *16*(10), 1525–1538. https://doi.org/10.1175/1520-0442-16.10.1525

Chadwick, R., Boutle, I., & Martin, G. (2013). Spatial patterns of precipitation change in CMIP5: Why the rich do not get richer in the tropics. *Journal of Climate*, *26*(11), 3803–3822. https://doi.org/10.1175/JCLI-D-12-00543.1

Deser, C., Phillips, A., Bourdette, V., & Teng, H. (2012). Uncertainty in climate change projections: the role of internal variability. *Climate Dynamics*, *38*(3–4), 527–546. https://doi.org/10.1007/s00382-010-0977-x

Diffenbaugh, N. S., & Scherer, M. (2011). Observational and model evidence of global emergence of permanent, unprecedented heat in the 20th and 21st centuries. *Climatic Change*, *107*(3), 615–624. https://doi.org/10.1007/s10584-011-0112-y

Falkner, R. (2016). The Paris Agreement and the new logic of international climate politics. *International Affairs*, *92*(5), 1107–1125.

Fuglestvedt, J., Rogelj, J., Millar, R. J., Allen, M., Boucher, O., Cain, M., et al. (2018). Implications of possible interpretations of "greenhouse gas balance" in the Paris Agreement. *Philosophical Transactions of the Royal Society A: Mathematical, Physical and Engineering Sciences*, *376*(2119), 20160445. https://doi.org/10.1098/rsta.2016.0445

Gillett, N. P., Arora, V. K., Zickfeld, K., Marshall, S. J., & Merryfield, W. J. (2011). Ongoing climate change following a complete cessation of carbon dioxide emissions. *Nature Geoscience*, *4*(2), 83–87. https://doi.org/10.1038/ngeo1047

Hallegatte, S. (2009). Strategies to adapt to uncertain climate change. *Global Environmental Change*, *19*(2), 240–247.

Hansen, J., Russell, G., Lacis, A., Fung, I., & Rind, D. (1985). Climate response times: Dependence on climate sensitivity and ocean mixing. *Science*, *229*(4716), 857–859.
Hawkins, E., & Sutton, R. (2012). Time of emergence of climate signals. *Geophysical Research Letters*, *39*, L01702. https://doi.org/10.1029/2011GL050087
Held, I. M., Winton, M., Takahashi, K., Delworth, T., Zeng, F., & Vallis, G. (2010). Probing the fast and slow components of global warming by returning abruptly to preindustrial forcing. *Journal of Climate*, *23*(9), 2418–2427. https://doi.org/10.1175/2009JCLI3466.1
Jacquet, J., & Jamieson, D. (2016). Soft but significant power in the Paris Agreement. *Nature Climate Change*, *6*(7), 643–646. https://doi.org/10.1038/nclimate3006
Keller, K., Bolker, B. M., & Bradfor, D. F. (2004). Uncertain climate thresholds and optimal economic growth. *Journal of Environmental Economics and Management*, *48*(1), 723–741.
Knight, J. R., Folland, C. K., & Scaife, A. A. (2006). Climate impacts of the Atlantic Multidecadal Oscillation. *Geophysical Research Letters*, *33*, L17706. https://doi.org/10.1029/2006GL026242
Mahlstein, I., Knutti, R., Solomon, S., & Portmann, R. W. (2011). Early onset of significant local warming in low latitude countries. *Environmental Research Letters*, *6*(3), 34009. https://doi.org/10.1088/1748-9326/6/3/034009
Manabe, S., Stouffer, R. J., Spelman, M. J., & Bryan, K. (1991). Transient responses of a coupled ocean–atmosphere model to gradual changes of atmospheric CO_2. Part I: Annual mean response. *Journal of Climate*, *4*(8), 785–818.
Marshall, J., Scott, J. R., Armour, K. C., Campin, J. M., Kelley, M., & Romanou, A. (2015). The ocean's role in the transient response of climate to abrupt greenhouse gas forcing. *Climate Dynamics*, *44*(7–8), 2287–2299. https://doi.org/10.1007/s00382-014-2308-0
Meehl, G. A., Stocker, T. F., Collins, W. D., Friedlingstein, P., Gaye, A. T., Gregory, J. M., et al. (2007). Global Climate Projections. In S. Solomon (Ed.), *Climate Change 2007: The Physical Science Basis. Contribution of Working Group I to the Fourth Assessment Report of the Intergovernmental Panel on Climate Change.* Cambridge, UK and New York: Cambridge University Press.
Meehl, G. A., Washington, W. M., & Collins, W. D. (2005). How much more global warming and sea level rise? *Science*, *307*(5716), 1769–1773. https://doi.org/10.1126/science.1106663
Meinshausen, M., Smith, S. J., Calvin, K., Daniel, J. S., Kainuma, M. L. T., Lamarque, J., et al. (2011). The RCP greenhouse gas concentrations and their extensions from 1765 to 2300. *Climatic Change*, *109*(1-2), 213–241. https://doi.org/10.1007/s10584-011-0156-z
Ricke, K. L., & Caldeira, K. (2014). Maximum warming occurs about one decade after a carbon dioxide emission. *Environmental Research Letters*, *9*(12), 124002. https://doi.org/10.1088/1748-9326/9/12/124002
Rogelj, J., Meinshausen, M., & Knutti, R. (2012). Global warming under old and new scenarios using IPCC climate sensitivity range estimates. *Nature Climate Change*, *2*(4), 248–253. https://doi.org/10.1038/nclimate1385
Rugenstein, M. A. A., Sedláček, J., & Knutti, R. (2016). Nonlinearities in patterns of long-term ocean warming. *Geophysical Research Letters*, *43*, 3380–3388. https://doi.org/10.1002/2016GL068041
Sen, P. K. (1968). Estimates of the regression coefficient based on Kendall's tau. *Journal of the American Statistical Association*, *63*(324), 1379–1389.
Solomon, S., Plattner, G.-K., Knutti, R., & Friedlingstein, P. (2009). Irreversible climate change due to carbon dioxide emissions. *Proceedings of the National Academy of Sciences*, *106*(6), 1704–1709.
Stouffer, R. (2004). Time scales of climate response. *Journal of Climate*, *17*(1), 209–217.
Sutton, R. T., Dong, B., & Gregory, J. M. (2007). Land/sea warming ratio in response to climate change: IPCC AR4 model results and comparison with observations. *Geophysical Research Letters*, *34*, L02701. https://doi.org/10.1029/2006GL028164
Thompson, D. W. J., Barnes, E. A., Deser, C., Foust, W. E., & Phillips, A. S. (2015). Quantifying the role of internal climate variability in future climate trends. *Journal of Climate*, *28*(16), 6443–6456. https://doi.org/10.1175/JCLI-D-14-00830.1
UNFCCC. (2015). Paris Agreement.
Wigley, T. M. L. (2005). The climate change commitment. *Science*, *307*(5716), 1766–1769.